Catalysis Communications 52 (2014) 65–71

Contents lists available at ScienceDirect

Catalysis Communications

journal homepage: www.elsevier.com/locate/catcom

Short Communication

On the composition of bimetallic near-surface alloys in the presence of oxygen and carbon monoxide

Jeffrey A. Herron, Manos Mavrikakis *

Department of Chemical and Biological Engineering, University of Wisconsin, Madison, WI, 53706, USA

ARTICLE INFO

Article history:
Received 21 August 2013
Received in revised form 15 October 2013
Accepted 17 October 2013
Available online 25 October 2013

Keywords:
Platinum alloys
Surface segregation
Density functional theory
Catalysis
Oxygen
CO

ABSTRACT

Periodic, self-consistent density functional theory calculations (GGA-PW91) are used to examine surface segregation in close-packed bimetallic Pt-overlayer alloy surfaces (Pt*/M, M = Au, Ag, Cu, Pd, Ir, Rh, Os, Ru, and Re) in different environments. In particular, we find that the thermodynamically stable surface termination in these Pt*/M alloys can be inverted from Pt-terminated in vacuum to M-terminated under exposure to oxygen (for an M that is more oxophilic than Pt). Interestingly, in many of these alloys, Pt is not driven into the bulk; rather it remains in the first subsurface layer where it enhances oxygen binding through a ligand interaction with the surface metal atoms. On the other hand, exposure to CO provides a much milder driving force for the surface composition inversion. To quantify segregation under catalytically relevant conditions, we constructed approximate phase diagrams for the PtRu system as a function of O_2 and CO chemical potential (temperature, pressure). The results show that the surface termination inverts with many orders of magnitude higher CO pressure than with O_2.

1. Introduction

The rational design of transition metal alloy catalysts with superior properties and reduced cost has been a goal for scientists and engineers for years. One class of alloys, so called near-surface alloys [1–3] have shown great promise in providing enhanced activity in a number of reactive systems [4–7]. However, experiments [8–12] and theory [8,13–18] have demonstrated that surface segregation may alter the surface composition of these materials, relative to the bulk, due to differences in the surface energy of the constituent metals [13,16,19], as well as each metal's affinity for adsorbates [2,8,12,14,18]. In particular, previous studies have examined adsorbate-induced segregation [14,18], whereby the surface is enriched in the metal which binds the adsorbate more strongly, overcoming the surface segregation energy. Therefore, the composition of the exposed surface of a catalyst particle is highly dependent on the interactions between the environment and the atoms in the nanoparticles. Pt near-surface alloys have shown to be attractive materials in a number of applications. They are active and cost-efficient oxygen reduction reaction (ORR) electrocatalysts [7,20], can be CO tolerant [6], and are active for the purification of hydrogen through preferential oxidation of CO [4]. A number of studies have investigated the fundamental ligand and strain effects [21–23] which modulate the catalytic properties of these alloys. Furthermore, the d-band model [24] has been used as a quantitative descriptor for these effects and has recently been applied to understand adsorbate-induced segregation [15].

As Pt surface alloy catalysts have shown high activity for a number of important reactions, we seek to understand how the composition of the near-surface region may change under reaction conditions. Herein, we report a first-principles, density functional theory (DFT-GGA) study of Pt surface alloy stability in the presence of O_2 or CO.

2. Methods

Periodic, self-consistent density functional theory calculations are performed using the Dacapo [25] total-energy code. A five-layer slab is periodically repeated in a super-cell geometry with a 2×2 surface unit cell. The slabs are repeated with at least five equivalent layers of vacuum between successive slabs. The top three layers are relaxed during optimization. Adsorption is only allowed on one of the two exposed surfaces. The electrostatic potential is adjusted accordingly [26], and the ionic cores are described by Ultrasoft Vanderbilt pseudopotentials [27]. The Kohn–Sham one-electron valence states are expanded in a basis of plane waves with kinetic energy below 25 Ry. The surface Brillouin zone was sampled at 18 special Chadi–Cohen k-points. The self-consistent exchange correlation energy is described within the generalized gradient approximation [28]. The self-consistent PW91 density is determined by iterative diagonalization of the Kohn–Sham Hamiltonian, Fermi population of the Kohn–Sham states ($k_BT = 0.1$ eV), and Pulay mixing of the resulting electron density [29]. All of the total energies were extrapolated to $k_BT = 0$ eV. Spin polarized calculations are employed when the oxygen coverage is 0.50 ML and above.

We study the close-packed surface, (111) for fcc metals and (0001) for hcp metals, of idealized near-surface alloys, retaining the crystal structure of the host metal, though we do not provide the surface

* Corresponding author.
E-mail address: manos@engr.wisc.edu (M. Mavrikakis).

1566-7367/$ – see front matter
http://dx.doi.org/10.1016/j.catcom.2013.10.021

designation, hereafter. All alloys include an equivalent monolayer of Pt (4 atoms in this case). The lattice constants for the host metals were optimized, using an ideal c/a ratio of 1.63. The PW91 optimized values (experimental values [30] in parentheses) are: Re 2.76 (2.76, c/a = 1.616), Ru 2.74 (2.72, c/a = 1.582), Os 2.73 (2.73), Ir 3.86 (3.84), Rh 3.83 (3.80), Pd 3.99 (3.89), Pt 4.00 (3.93) Au 4.18 (4.07), Ag 4.14 (4.09), Cu 3.66 (3.61), all values are in Å.

Adsorption of atomic O and CO was studied on Pt*/Ru while permuting the positions of the Pt and Ru atoms within the top three layers of the slab (see Fig. 1). The composition of the surfaces is denoted from the outermost layer to innermost layer, from left to right, with each layer separated by a slash. The overlayer (left most) is also denoted with an asterisk, and the bulk composition corresponds to the last layer listed. For example, Fig. 1a, b, and c would be denoted Pt*/Ru, $Pt_3Ru^*/PtRu_3/Ru$, and Ru*/Pt/Ru, respectively. The 4 Pt atoms were exchanged between the first and second layers, while maintaining contiguous Ru layers in the third, fourth and fifth layers. Then, the Pt atoms were exchanged between the second and third layers, while maintaining contiguous Ru layers in the first, fourth and fifth layers. We did not investigate having Pt simultaneously in the first and third layers. We note that there are multiple, distinct, ways to generate surfaces with a particular layer-by-layer stoichiometry sequence. For example, for the $Pt_3Ru^*/PtRu_3/Ru$ surface, it can be arranged such that the Pt atom in the second layer rests below a surface hollow site with 3 Pt atoms, or one can arrange the atoms such that the underlying Ru rests below this site (see supporting information for more details). However, for the sake of simplicity in reporting, we only report the most stable configuration for each distinct layer-by-layer stoichiometry sequence. The PtRh, PtIr, and PtRe systems were modeled using a five layer slab with a Pt-overlayer and with Pt atoms being permuted between the second and third layers (Fig. 1a, c, d, and e). For all other alloys, the systems were studied by permuting the position of a contiguous Pt layer within the slab: as the first layer (overlayer), the second layer, or as the third layer (Fig. 1a, c, and e). All of these systems were studied at 0.25, 0.50, 0.75, and 1 ML coverage of the adsorbates (O or CO).

Vibrational frequencies for gas phase O_2, gas phase CO, adsorbed O, and adsorbed CO are calculated by numerical differentiation of forces using a second-order finite difference approach with a step-size of 0.015 Å [31]. The Hessian matrix is mass-weighted and diagonalized to yield the frequencies and normal modes. The vibrational entropies of these species are derived from the vibrational frequencies using a harmonic oscillator approximation. The vibrational frequencies of adsorbed O and CO species are calculated on Pt(111) at ¼ ML coverage and are assumed, as a first approximation, to be independent of the material composition of the surface and the surface coverage of adsorbates. Therefore, we use these values for all surfaces. Furthermore, the vibrational entropy of the higher coverage states is calculated by multiplying the lower coverage result, i.e. the entropy with ½ ML of O is two times the entropy of the ¼ ML result.

Phase diagrams for the O-Pt*/Ru system were derived by calculating the grand potential (Ω) for every system with the equation $\Omega = E_{system} - E_{Pt^*/Ru} - N_O\mu_O - TS$, where E_{system} is the total energy of a surface with N_O O atoms adsorbed, $E_{Pt^*/Ru}$ is the total energy of the clean Pt*/Ru system, μ_O is the chemical potential of O, T is the absolute temperature (300 K), and S is the vibrational entropy of the system. The chemical potential of O is related to the chemical potential of O_2 as $\mu_O = \frac{1}{2}\mu_{O2}$, with $\mu_{O2} = \mu'_{O2} + E_{O2} - TS_{O2}$, where E_{O2} is the total energy of gas phase O_2 that was calculated using DFT, and S_{O2} is the vibrational entropy of gas phase O_2. Assuming that O_2 is an ideal gas, $\mu'_{O2} = k_BT \ln P/P^\circ$, where k_B is the Boltzmann constant, P is the O_2 pressure, and P° is 1 atm. Similarly, the phase diagram for the Pt*/Ru–CO system was calculated from $\Omega = E_{system} - E_{Pt^*/Ru} - N_{CO}\mu_{CO} - TS$, with $\mu_{CO} = \mu'_{CO} + E_{CO} - TS_{CO}$ and $\mu'_{CO} = k_BT \ln P/P^\circ$. We note that these phase diagrams are simplified models and are meant to illustrate qualitative differences between the systems [31,32].

3. Results and discussion

3.1. Oxygen adsorption on Pt*/Ru

The stability of the Pt*/Ru system was assessed as a function of oxygen coverage while systematically exchanging the positions of the Pt and Ru atoms between the first two layers. The stability of each $Pt_xRu_{4-x}^*/Pt_{4-x}Ru_x/Ru$ system at varying O coverage (x = 0, 1, 2, 3 or 4), referenced to the Pt*/Ru system at a given O coverage (negative numbers are more stable than Pt*/Ru), is shown in Fig. 2a.

From these results we note a few effects. First, in vacuum, exchanging 0.25 ML of Ru from the subsurface with surface Pt is energetically unfavorable (+0.48 eV), in agreement with previous theoretical studies [13,14]. However, in the presence of oxygen, this exchange becomes thermodynamically favorable at all O-coverages tested. The reason for this behavior is that Ru has a much stronger affinity for oxygen than does Pt. In particular, previous DFT studies have calculated the binding energy of O at 0.25 ML coverage on Pt(111) as −3.87 eV [33], while it is −5.43 eV on Ru(0001) [34]. At 0.25 ML oxygen coverage, it is most favorable to have 0.25 ML coverage of Ru in the surface. At 0.50 ML oxygen coverage, 0.75 ML Ru coverage is favored, and at 0.75 ML oxygen coverage and higher, a Ru overlayer is preferred. Monte Carlo studies of oxygen adsorption on a $Pt_{50}Ru_{50}$ alloy have shown a linear increase in surface Ru with oxygen coverage, in qualitative agreement with our results [14].

To illustrate the effect of oxygen adsorption on surface segregation under realistic conditions, we calculated phase diagrams for the O–(Pt*/Ru) system. In Fig. 2b, we show the phase diagram of the O–(Pt*/Ru) system without allowing for surface segregation, whereas Fig. 2c shows the phase diagram with allowing for surface segregation. First, we note that completely inverting the surface termination (i.e. exchanging all Pt atoms with subsurface Ru atoms) is thermodynamically driven at 10^{-23} atm (8×10^{-21} torr) O_2 pressure at 300 K. Also, the O coverage for the segregated system is significantly higher than the Pt*/Ru system at a given pressure and temperature. A full monolayer of O is stable in the segregated system, at 300 K, with 87 orders of magnitude lower O_2 pressure than in the unsegregated system. We caution the reader that these results reflect only system thermodynamics. The

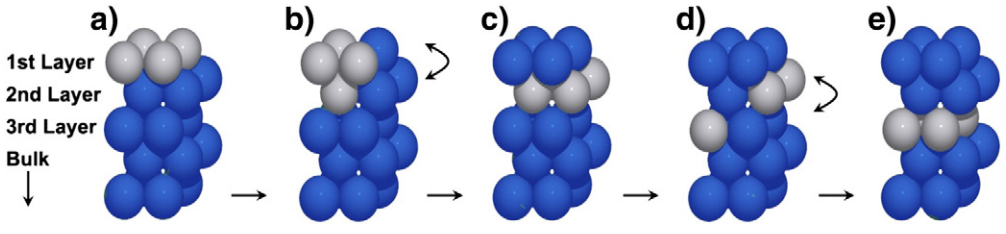

Fig. 1. Illustration of unit-cell slab models used, with Pt atoms shown in silver and second metal (e.g. Ru) shown in blue. In a) contiguous Pt overlayer, b) Pt exchange with second layer, c) contiguous Pt layer in 2nd layer, d) Pt exchange with third layer, e) and contiguous Pt layer in 3rd layer.